Acta Pharmaceutica Sinica B 2023;13(9):3919–3929

Chinese Pharmaceutical Association
Institute of Materia Medica, Chinese Academy of Medical Sciences

Acta Pharmaceutica Sinica B

www.elsevier.com/locate/apsb
www.sciencedirect.com

ORIGINAL ARTICLE

Characterization of the depsidone gene cluster reveals etherification, decarboxylation and multiple halogenations as tailoring steps in depsidone assembly

Jiafan Yang[a,b], Zhenbin Zhou[a,b], Yingying Chen[a], Yongxiang Song[a,b,*], Jianhua Ju[a,b,*]

[a]*CAS Key Laboratory of Tropical Marine Bio-resources and Ecology, RNAM Center for Marine Microbiology, Guangdong Key Laboratory of Marine Materia Medica, South China Sea Institute of Oceanology, Chinese Academy of Sciences, Guangzhou 510301, China*
[b]*University of Chinese Academy of Sciences, Beijing 110039, China*

Received 13 February 2023; received in revised form 17 April 2023; accepted 12 May 2023

KEY WORDS

Depside and depsidone;
Polyketide synthase;
Tailoring enzymes;
Multiple-halogenated;
Antibacterial activity

Abstract Depsides and depsidones have attracted attention for biosynthetic studies due to their broad biological activities and structural diversity. Previous structure–activity relationships indicated that triple halogenated depsidones display the best anti-pathogenic activity. However, the gene cluster and the tailoring steps responsible for halogenated depsidone nornidulin (**3**) remain enigmatic. In this study, we disclosed the complete biosynthetic pathway of the halogenated depsidone through *in vivo* gene disruption, heterologous expression and *in vitro* biochemical experiments. We demonstrated an unusual depside skeleton biosynthesis process mediated by both highly-reducing polyketide synthase and non-reducing polyketide synthase, which is distinct from the common depside skeleton biosynthesis. This skeleton was subsequently modified by two in-cluster enzymes DepG and DepF for the ether bond formation and decarboxylation, respectively. In addition, the decarboxylase DepF exhibited substrate promiscuity for different scaffold substrates. Finally, and interestingly, we discovered a halogenase encoded remotely from the biosynthetic gene cluster, which catalyzes triple-halogenation to produce the active end product nornidulin (**3**). These discoveries provide new insights for further understanding the biosynthesis of depsidones and their derivatives.

*Corresponding authors.
E-mail addresses: songx@scsio.ac.cn (Yongxiang Song), jju@scsio.ac.cn (Jianhua Ju).
Peer review under the responsibility of Chinese Pharmaceutical Association and Institute of Materia Medica, Chinese Academy of Medical Sciences.

https://doi.org/10.1016/j.apsb.2023.05.036

1. Introduction

Depsidones and depsides (DEPs) are the classic natural products widely produced by fungi, lichens, and plants[1–3]. To date, more than 100 DEPs have been reported and exhibited extensively varying bioactivities such as anti-microbial, anti-tumor, anti-oxidant, anti-virus, and enzyme inhibitor activities[1,4–7]. DEPs consist of two 2,4-dihydroxybenzoic acid rings linked to each other by both ether and ester bonds. They are usually highly halogenated in fungi, which is one means by which DEPs chemical diversity is enriched. Previously structure–activity relationships (SARs) showed that the anti-infective activities of the highly halogenated depsidones (nornidulin (**3**) and emeguisin A (**10**)) are much stronger than the depside precursors (agonodepside A (**1**) and unguidepside A (**2**))[8] (Fig. 1). Although the first depsidone, nidulin (**4**), has been reported in 1949[9], the biosynthetic gene clusters (BGCs) and detailed tailoring enzymes responsible for generating these interesting bioactive compounds in fungi have not yet been elucidated.

Initiatives to understand DEPs and related biosynthetic machineries have lagged far behind the discovery of their analogues and semi-synthetic approaches to chemical derivatives[1,6,13,14]. It was not until 2018 that Andrew M. Piggott and co-workers[7] conducted a precursor-directed biosynthesis of depsidones. These studies were inspired by their hypothesis that DEPs biosynthesis employs a single polyketide synthase (PKS) that carries out the assembly of the acyclic core scaffold and converges the two aromatic rings to yield a depside. Recently, three interesting biosynthesis cases for depside skeleton assembly have been elucidated in fungi (Scheme 1, Routes A–C)[10–12]. Notably, all of them need only one non-reducing polyketide synthase (nrPKS). Unusually, in routes A and B, the depside bond formation is proved to be catalyzed by the starter-unit acyltransferase (SAT) domain (Scheme 1, Routes A–B)[10,12]. However, it is still unclear how unguidepside A (**2**) converts to nornidulin (**3**), and whether the multiple halogenated in DEPs is catalyzed by one or multiple enzymes. Identifying novel tailoring enzymes from nature is vital for generating novel bioactive compounds *via* metabolic engineering to modify the biosynthetic pathways for drug development[15]. Thus, further characterization of tailoring enzymes during DEPs assembly would boost our understanding of the biosynthetic pathway of this vital natural product family. In this study, we discovered that the bicyclic depside skeleton formation in DEPs involved two PKSs (Scheme 1, Route D). In addition, the tailoring steps of etherification, decarboxylation, and multiple halogenations of DEPs were also investigated in *Aspergillus* sp. SCSIO SX7S7.

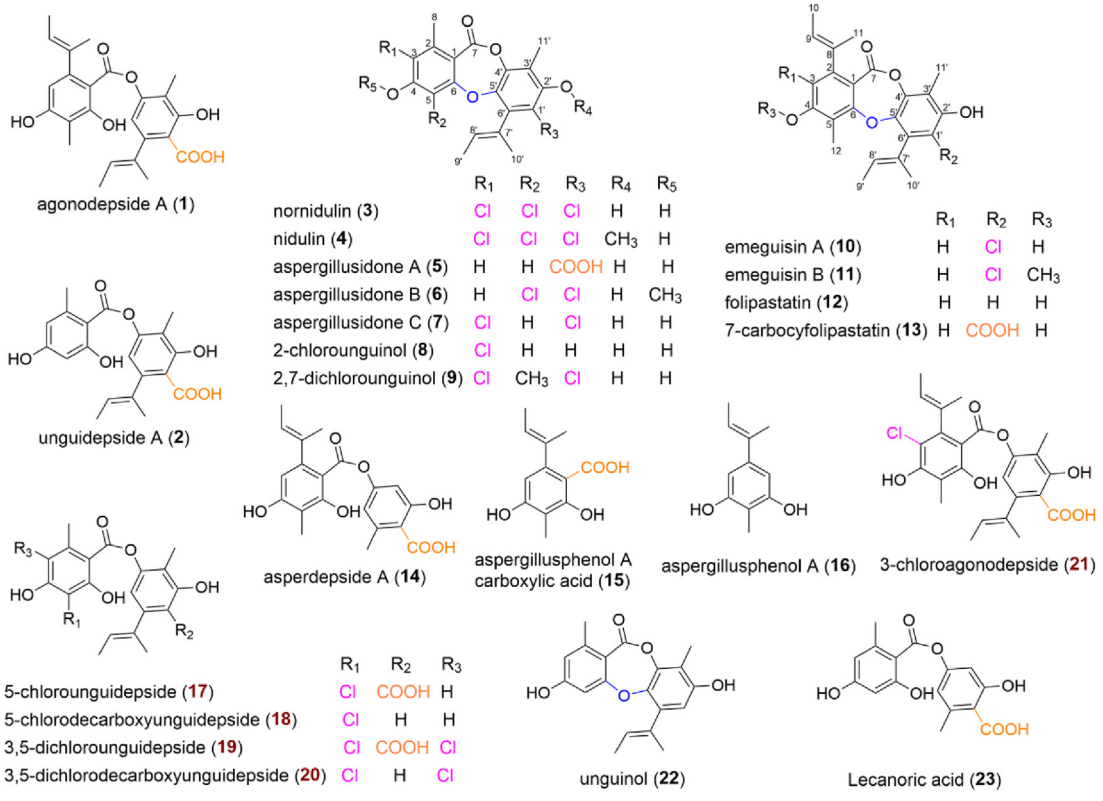

Figure 1 Compounds **1**–**16** were previously isolated from the *Aspergillus* sp. SCSIO SX7S7[8]. Compounds **17**–**22** were isolated in this study from its mutants. The new compounds were marked in red. Compound **23** was detected by LC–MS analysis.

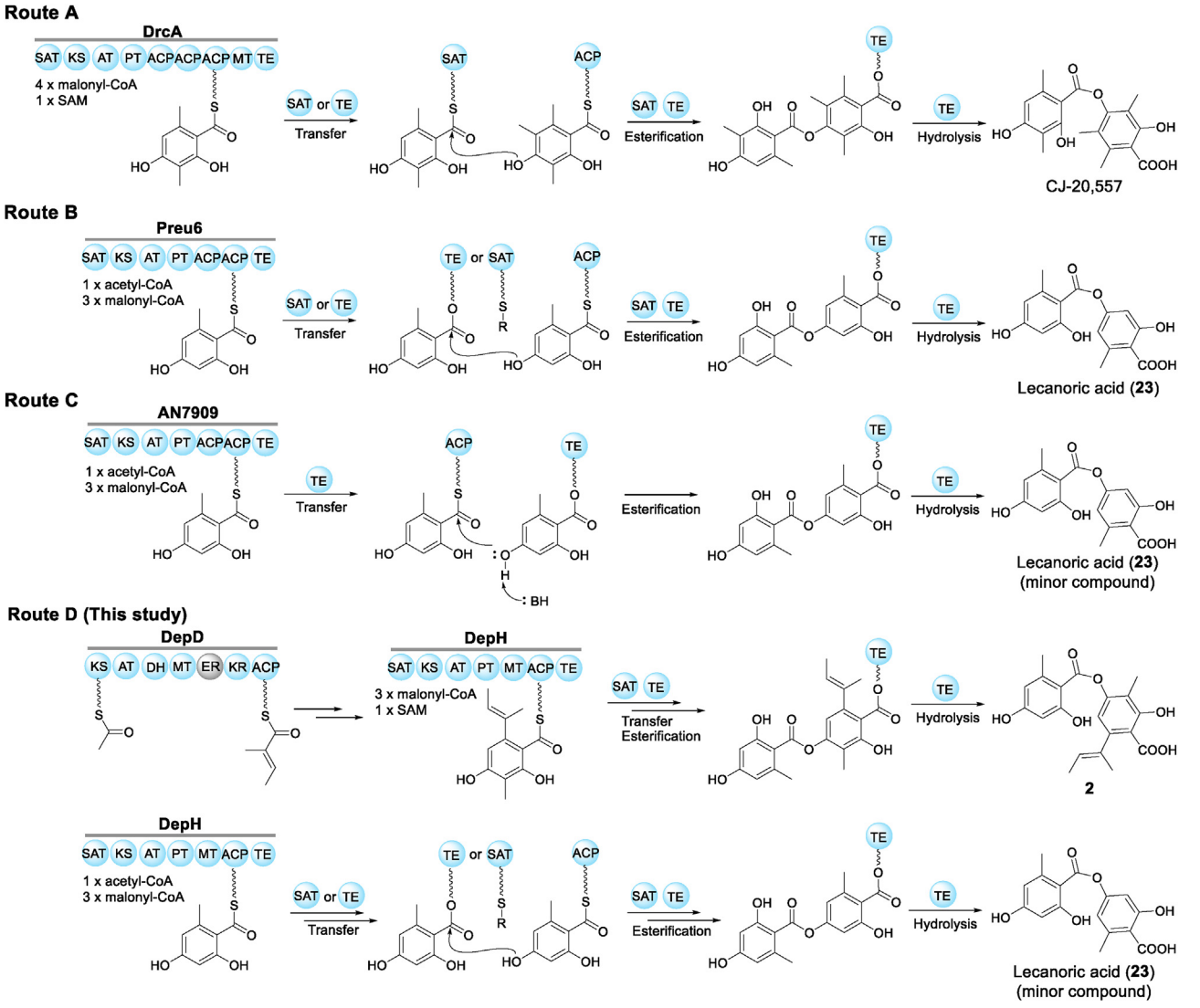

Scheme 1 Biosynthetic models for depside formation. Routes A−C are previously reported cases in which the depside skeleton was formed by a single PKS[10−12]. Route D is the proposed formation of precursors **2** and **23** in this study, compound **2** was formed by two PKSs.

2. Results and discussion

2.1. Identification of the dep gene cluster unveils the formation of precursor unguidepside A (2) requiring both hrPKS and nrPKS

In our previous chemical investigations, a series of tricyclic depsidones and bicyclic depsides were obtained from the coral-derived fungus *Aspergillus* sp. SCSIO SX7S7 (Fig. 1)[8]. The SARs analyses showed that the existence of the heptacyclic ring is crucial to anti-pathogen activities and that tailoring steps such as decarboxylation and multiple halogenation can enhance antimicrobial activities[8].

To clarify the biosynthetic production mechanisms affording DEPs, whole-genome sequencing of *Aspergillus* sp. SCSIO SX7S7 was performed using Illumina technology and assembled into a total of 53 scaffolds (~26.6 Mb in size). AntiSMASH analyses[16] showed that the genome of SCSIO SX7S7 encodes at least 49 secondary metabolite (SM) BGCs, including 6 highly reducing polyketide synthases (hrPKS), 4 nrPKS, and 2 nrPKS and hrPKS hybrid BGCs (Supporting Information Table S1). Bioinformatically, the nrPKS of hybrid BGC in scaffold 11 showed 51% identical to Preu6 which was responsible for lecanoric acid (**23**) (Fig. 1, Scheme 1, Route B)[12]. However, other candidate PKSs do not have the potential to produce DEPs based on the homology analysis (Table S1). Meanwhile, in this hybrid BGC (Table 1, Fig. 2A), the domain architecture of hrPKS (DepD) is ketosynthase (KS)-acyltransferase (AT)-dehydratase (DH)-*C*-methyltransferase (cMT)-enoylreductase (ER)-ketoreductase (KR)-acyl carrier protein (ACP). Moreover, the nrPKS (DepH) contains a domain architecture of SAT-KS-AT-PT (Product Template)-cMT-TE. To critically evaluate the BGCs of interest, we inactivated the possible nrPKS distributed in the scaffold 11 based on our previously reported CRISPR-Cas9 gene disruption system to identify the key enzymes responsible for constructing the DEPs skeleton[17]. Expectedly, inactivation of the nrPKS (*depH*) in scaffold 11 completely abolished the production of DEPs (Fig. 2B, v). Thus, we reasoned that the *depH*-containing cluster is responsible for DEP biosynthesis in *Aspergillus* sp. SCSIO SX7S7 (Fig. 2A). Accordingly, this cluster was designated as the *dep* cluster, and subsequent studies revealed that it contains

Table 1 The deduced functions of ORFs from the *dep* gene cluster in SCSIO SX7S7.

Orfs	Proposed function, origin	ID/SI[a]	Protein homologue and origin
−2	Serine/threonine kinase, Vhs1	36/51	(Q03785.1): *Saccharomyces cerevisiae* S288C
−1	Putative protein	—	—
depA	Serine/threonine kinase, Prp4	71/78	(Q07538.2): *Schizosaccharomyces pombe* 972 h-
depB	Translation machinery-associated protein	58/77	(Q4SUE2.1): *Tetraodon nigroviridis*
depC	Putative protein	66/74	(XP_026605900.1): *Aspergillus mulundensis*
depD	HrPKS, CdmE (KS-AT-DH-cMT-ER-KR-ACP)	32/50	(A0A3G9GQ29.1): *Talaromyces verruculosus*
depE	Putative protein	49/62	(XP_025519284.1): *Aspergillus piperis* CBS 112811
depF	Decarboxylase, YanB	37/54	(G3Y417.1): *Aspergillus niger* ATCC 1015
depG	Cytochrome P450 monooxygenase, Atr2	33/52	(A0A8F4SN83.1): *Stereocaulon alpinum*
depH	NrPKS, Preu6(SAT-KS-AT-PT-MT-ACP-TE)	51/67	(P9WET2.1): *Preussia isomera*
depI	Putative protein	55/70	(XP_035339546.1): *Talaromyces rugulosus*
depJ	Dioxygenase	36/49	(P31019.1): *Pseudomonas* sp. EST1001
depK	Cytochrome P450 monooxygenase, AneD	35/54	(A0A1L9WUS5.1): *Aspergillus aculeatus* ATCC 16872
depL	Putative protein	88/94	(XP_662543.1): *Aspergillus nidulans* FGSC A4
depM	3-Oxoacyl-reductase, FabG	35/52	(Q9X248.1): *Thermotoga maritima* MSB8
1	Putative protein	91/93	(XP_026605893.1): *Aspergillus mulundensis*
2	Putative protein	89/95	(XP_662535.1): *Aspergillus nidulans* FGSC A4

[a]ID/SI: Identity/Similarity.

15 genes altogether (deposited as GenBank accession number OP889148, Table 1). Another hrPKS gene, *depD*, was further inactivated, and as expected, the mutant strain failed to accumulate any DEPs (Fig. 2B, ii).

To obtain the precursor derived from the *dep* cluster, we performed heterologous expression and constructed two plasmids that contain *depD* and *depH* for the protoplast transformation to the model fungus *A. nidulans* A1145[18]. As a result, precursor **1/2** could be afforded only when the two PKS genes were expressed together (Fig. 2C). Meanwhile, the trace amounts of **23** (Fig. 1) could also be detected by LC−MS analyses either in the *depD* and *depH* coexpressing strain or *depH* expressing alone strain, but not in *depD* expressing alone strain (Supporting Information Fig. S6). Thus, we deduced that DepH could catalyze the formation of **23** only, and the formation of **1/2** requires both two PKSs involved. Phylogenetic analysis of the SAT and TE domains of DepH showed that they are clustered with Preu6, an nrPKS is capable of catalyzing the formation of **23** (Supporting Information Fig. S22) suggesting that the formation of depsides **2** and **23** is likely consistent with that of Preu6 (Scheme 1, Routes B, D)[12]. Interestingly, the formation of unguidepside A (**2**) requires a hrPKS DepD, in which the ER domain may be malfunctional based on the observed "DSLG" NADPH binding site instead of the canonical "GGXG" site through the alignment of DepD ER domain with that in other fungal hrPKSs (Supporting Information Fig. S23). Thus, DepD could generate 1-methyl-1-propenyl unit for nrPKS DepH (Scheme 1, Route D), which differs from previous reports that the formation of depside requires one nrPKS only (Scheme 1, Routes A−C).

2.2. *In vivo and in vitro experiments reveal the cytochrome P450 monooxygenase DepG catalyzes the installation of ether bond*

To extend our understanding of DEPs biosynthesis, we next analyzed the genes neighboring *depD* and *depH* within the *dep* cluster. We envisioned that some of these genes might be responsible for catalyzing key tailoring steps *en route* to the depsidones. We first inactivated three putative oxidase genes (*depG*, *depJ*, and *depK*) in the *dep* cluster, which is thought to possibly catalyze the installation of ether bonds in the depsidones. Compared with the wild-type (WT) producer, HPLC-DAD finger spectra and (+)-LC−HR-ESI-MS analyses of the three inactivated mutants, revealed that the Δ*depG* mutant produced five new peaks (Fig. 2B, iv, **17**−**21**), whereas the Δ*depJ* and Δ*depK* mutants produced an SM profile consistent with the WT producer (Supporting Information Fig. S21). (+)-LC−HRESIMS analysis of the Δ*depG* mutant product profile showed that the molecular weights of the main products were 2 Da greater than their WT counterparts, suggesting that cytochrome P450 monooxygenase DepG likely drives the installation of the 6-*O*-5′ biaryl ether linkage in the depsidones. Furthermore, large-scale fermentation, isolation, and identification of the Δ*depG* products revealed that this mutant no longer produced the 6/8/6 skeleton of the DEPs, but rather generated new depsides **17**−**21** devoid of the biaryl ether linkage (Fig. 1). The structures of **17**−**21** were carefully elucidated by extensive HRESIMS, and 1D and 2D NMR data analysis (Supporting Information Fig. S1, Tables S7−S8).

In support of these findings, we also performed feeding experiments using the *A. nidulans* A1145-*depG* (AN-*depG*) strain. When compounds **2** and **21** were fed to AN-*depG*, depsidones **5** and **21a** could be readily observed. These data confirmed that DepG carries out biaryl ether bond installation in the DEPs (Fig. 3A). Since DepG is membrane-bound, *in vitro* characterization of such an enzyme remains challenging (Supporting Information Fig. S5). Herein, we prepared a high concentration of microsomal fraction of the strain AN-*depG*. Following the incubation of 0.1 mmol/L **2** with 420 μL microsomal DepG source, 2 mmol/L NADPH, and 100 mmol/L NaCl for 12 h, a putative bio-transformation product could be detected in HPLC-DAD analyses (Fig. 3B). The identity of the putative DepG product corresponded strongly to the compound **5** standard further validating that stand-alone DepG is able to catalyze the formation of ether bonds in the DEPs. In addition, precursors-direct biosynthesis might be possible to generate depsidone congeners for the development of anti-infectious agents with high activity.

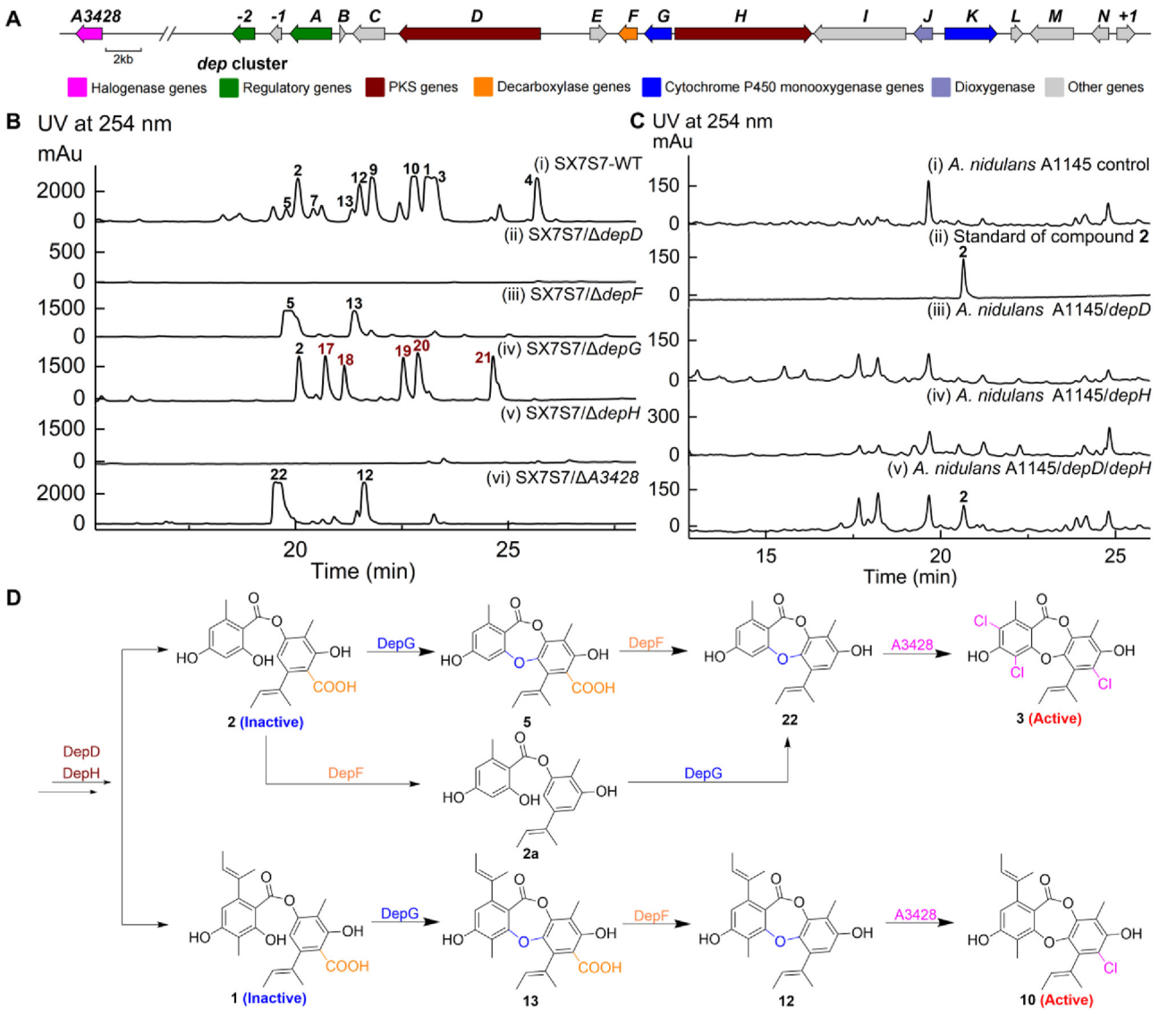

Figure 2 Biosynthetic gene cluster of DEPs, HPLC profiles, and proposed biosynthetic pathway of DEPs. (A) Gene cluster of DEPs; (B) HPLC profiles of the wide type strain and mutants of SCSIO SX7S7; (C) HPLC profiles of the PKS heterologous expression in *A. nidulans* A1145; (D) The proposed late-stage biosynthetic pathway of depsidones **3** and **10** based on biochemical and genetic evidence.

2.3. In vivo and in vitro characterization of DepF as an efficient decarboxylase with promiscuous activity

Previous SARs showed that decarboxylation of depsidones enhances their anti-pathogenic activity[8]. Bioinformatic analysis of *depF* showed that it likely encodes for an amidohydrolase superfamily protein. This family has previously been shown to catalyze decarboxylation in diphenyl ethers[19]. Thus, we envisioned that DepF might be responsible for the C-1′ decarboxylation in DEPs[19–21]. Notably, most members of this family require divalent metals for catalytic function. HPLC-DAD analyses showed that the main products of the Δ*depF* mutant were compounds **5** and **13** containing the C-1′ carboxy moiety (Fig. 2B, iii). Combined (+)-LC−HRESIMS analyses (Supporting Information Fig. S2) with the Δ*depF* product profile confirmed that DepF catalyzes decarboxylation during DEP assembly. To validate the function of DepF, intron-free *depF* was cloned, then overexpressed and purified from *Escherichia coli* BL21 (DE3) (Supporting Information Fig. S4). As we expected, after an incubation of 20 μmol/L DepF with 100 μmol/L **2** and **5** for 2 h, the expectant conversions of **2** to **2a** and **5** to **22** could be readily detected (Fig. 4A). (+)-LC−HRESIMS revealed the presence of both **2a** and **22** as decarboxylated products (Supporting Information Fig. S7), providing clear evidence for the decarboxylation of DEPs by DepF. Interestingly, DepF incubations containing **2** or **5**, along with 10 mmol/L EDTA, were found to yield the products **2a** and **22**, respectively, suggesting that DepF might not require metal ions to decarboxylate DEP substrates. Using the optimal reaction conditions, we determined the kinetic constants for DepF. The K_m and k_{cat} values for DepF conversion of **5** to **22** were found to be 23.5 μmol/L and 4298.5/min respectively, and 10.3 μmol/L and 184.8/min for the conversion of **2** to **2a** (Fig. 4B). Thus, the optimum natural substrate for DepF was found to be depsidone **5**, and DepF was also found to have excellent catalytic activity.

Enzyme promiscuity plays an important role in developing diversified products[22,23]. Owing to the efficient catalytic activity of

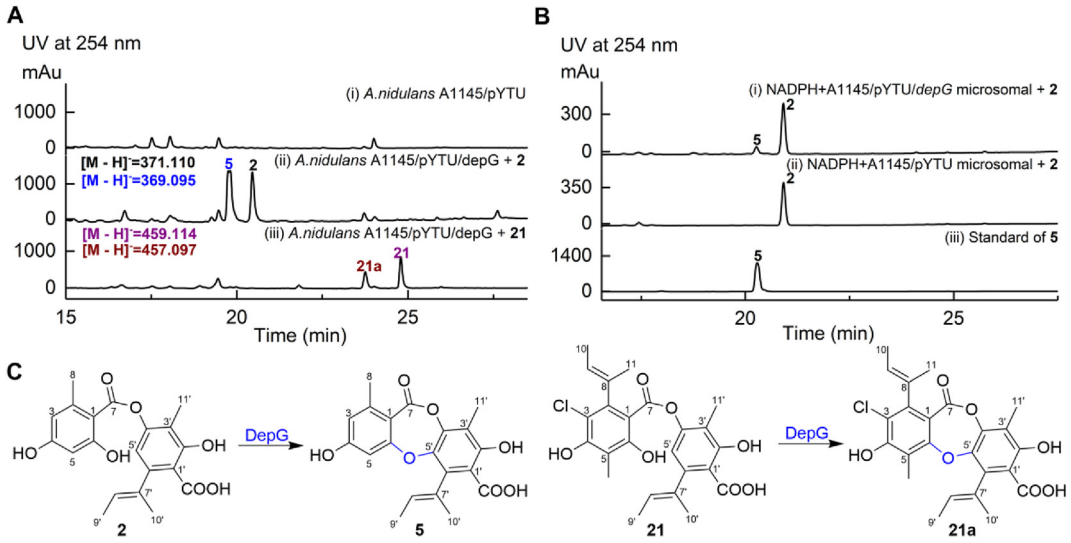

Figure 3 *In vivo* and *in vitro* analysis of the cytochrome P450 monooxygenase DepG. (A) *In vivo* biotransformation of DEP precursors in *A. nidulans* A1145/*depG* using **2** and **21** as the substrates; (B) HPLC traces of the DepG-catalyzed reactions using **2** as the substrate; (C) The verified substrates and reactions catalyzed by DepG.

DepF, the substrate range of this enzyme was also performed. When compound **15** was used as a substrate, the expected products of compound **16** could be detected by the trace of HPLC (Fig. 4A). Additionally, K1115A (**24**) obtained from one strain of *Streptomyces* sp. by our team was also used to test the substrate scope of DepF. Coincubation of **24** with DepF led to the formation of the expected product, 1,6-dihydroxy-8-propylanthraquinone (**24a**) (Fig. 4A), which was further confirmed by LC−MS (Fig. S7), indicating that DepF could also catalyze the decarboxylation of anthraquinones (Fig. 4C). Taken together, above results revealed that DepF might catalyze the decarboxylation during DEPs biosynthesis with a remarkable substrate scope, including on-pathway intermediates and other sources of compounds.

2.4. A3428 is a remotely encoded flavin-dependent halogenase capable of catalyzing multiple-halogenation within DEPs biosynthesis

The discovery of many highly halogenated DEPs indicates the existence of a halogenase that might be responsible for multiple halogenations. To date, biochemical characterization of flavin-dependent halogenase which could catalyze the formation of multi-halogenated natural products in fungi is rare. It is of great significance to characterization of such an enzyme which might convert DEPs to highly halogenated DEPs.

Bioinformatics analyses were carried out to identify candidate halogenase genes within the *dep* cluster. Interestingly, no such genes were found based on gene function annotations and gene disruption results (Table 1, Fig. S21). Therefore, we speculated that the gene encoding halogenase is located outside of the *dep* cluster. To identify the target halogenase involved in DEPs biosynthesis, we searched the reports on ortho halogenation of phenolic hydroxy group and found two flavin-dependent halogenases, RadH and AclH, responsible for radicicol and aspirochlorine halogenation, respectively[24,25]. Upon comparison of RadH and AclH with all of the SX7S7 encoded putative proteins, a candidate A3428 that was 47% identical to RadH and 52% identical to AclH was found (Supporting Information Fig. S12). However, other proteins were less than 35% identical. Notably, *A3428* does not appear to be a component of any previously identified SM gene clusters within SCSIO SX7S7. To validate A3428 as the halogenase responsible for DEPs biosynthesis, we inactivated *A3428* with CRISPR-Cas9 system. As expected, the mutant mainly accumulated compounds **12** and **22** as determined by HPLC-DAD analysis (Fig. 2B, vi). At the same time, compounds **5** and **13** could also be detected in (−)-LC−HRESIMS analyses, instead of the typical halogenated DEPs (Supporting Information Fig. S3). Taken together, these results confidently demonstrated that flavin-dependent halogenase A3428, a remotely encoded biosynthetic tailoring enzyme, is essential for the halogenation of DEPs.

To obtain direct *in vitro* evidence for the biochemical functions of A3428, an approach similar to that taken for DepF was pursued. The intron-free *A3428* was cloned from the cDNA and heterologously overexpressed in *E. coli* BL21 (DE3) (Supporting Information Fig. S4). The resulting enzyme was sufficiently pure for *in vitro* enzyme assays with various substrates. Incubations of **2** with 15 μmol/L A3428, 2.5 mmol/L NADH, and 25 mmol/L $MgCl_2$ for 12 h afforded none of the putative products as determined by HPLC. However, upon the addition of 20 μmol/L of Fre (*E. coli* flavin reductase[26]), monochlorinated **17** and dechlorinated **2b** were detected in the 4 and 8 h reactions, respectively (Fig. 5A, i−iii). The identities of putative **17** and **2b** were further confirmed by (−)-LC−HRESIMS analyses (Supporting Information Fig. S8). Thus, we demonstrated that the activity of A3428 is dependent upon the presence of a reductase partner. Further investigations revealed that A3428 could accept a range of substrates. With the exception of **2**, compounds **12** and **22** could be processed by A3428, and their polychlorinated products could be easily detected by HPLC (Fig. 5A, iv−x) and LC−MS (Supporting Information Fig. S9). On the other hand, when $MgCl_2$ was replaced by KBr and KI, we found that putative A3428 products could only be detected in the KBr system. KI-containing reactions failed to yield any discernible halogenated derivates (Supporting Information Fig. S10). Brominated DEPs were further confirmed by LC−MS analysis (Supporting Information Fig. S11). These data indicated that A3428 could employ either $MgCl_2$ or KBr to afford assorted

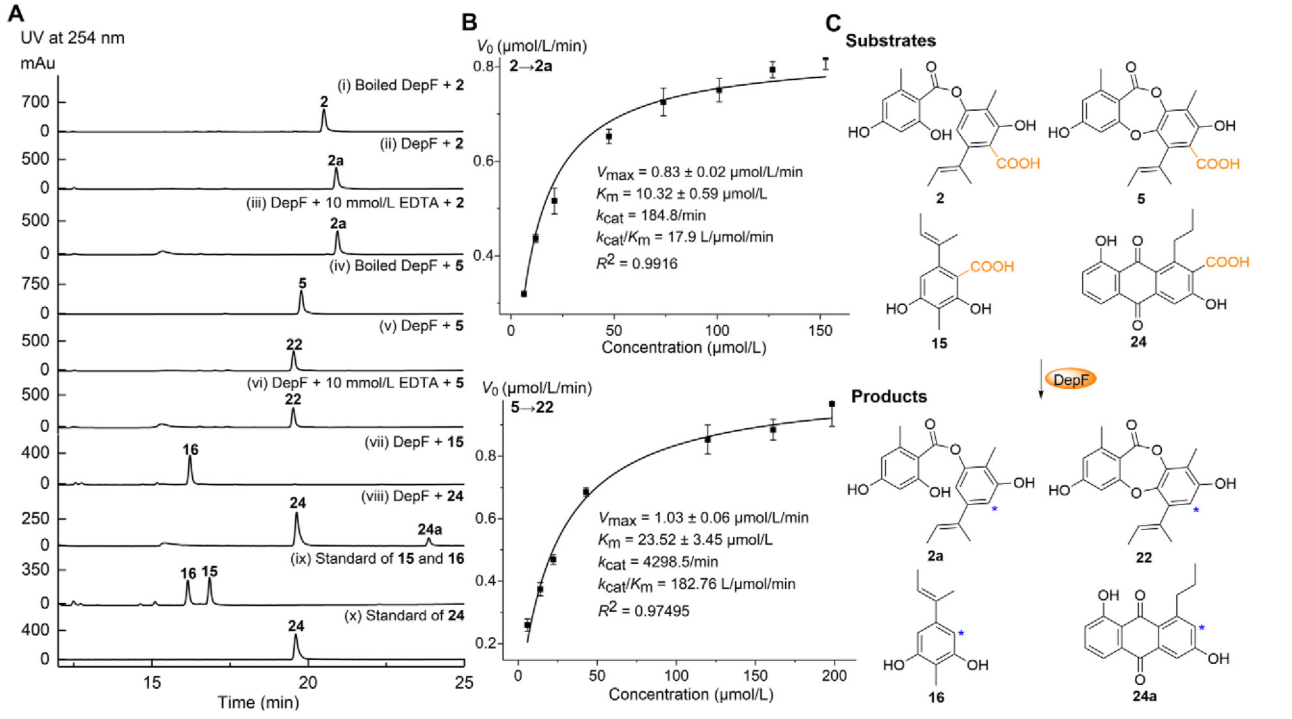

Figure 4 Biochemical characterization of DepF. (A) *In vitro* analyses of DepF using **2**, **5**, **15**, and **24** as substrates; (B) Kinetic constants for DepF-catalyzed reactions, using **2** and **5** as substrates; The inset numbers represent the determined kinetic constant values. Error bars are exhibited as SEM; (C) The verified substrates and reactions catalyzed by DepF. The asterisk mark indicates the decarboxylation position.

DEPs differing in their halogenation patterns. Collectively, we confirmed that A3428 as a flavin-dependent halogenase could finalize the installation of different halogen atoms during DEPs biosynthesis with broad substrate scope and represent an important advance that will likely enable enhanced access to new DEPs as potential new compounds or drug leads.

2.5. *Antibacterial activity assays*

Finally, we investigated the antimicrobial activities of the new depsides **17**−**21** (Fig. 1). Compounds **18** and **20** were both found to possess antibacterial activities against a series of Gram-positive pathogens with minimum inhibitory concentrations (MICs) span-

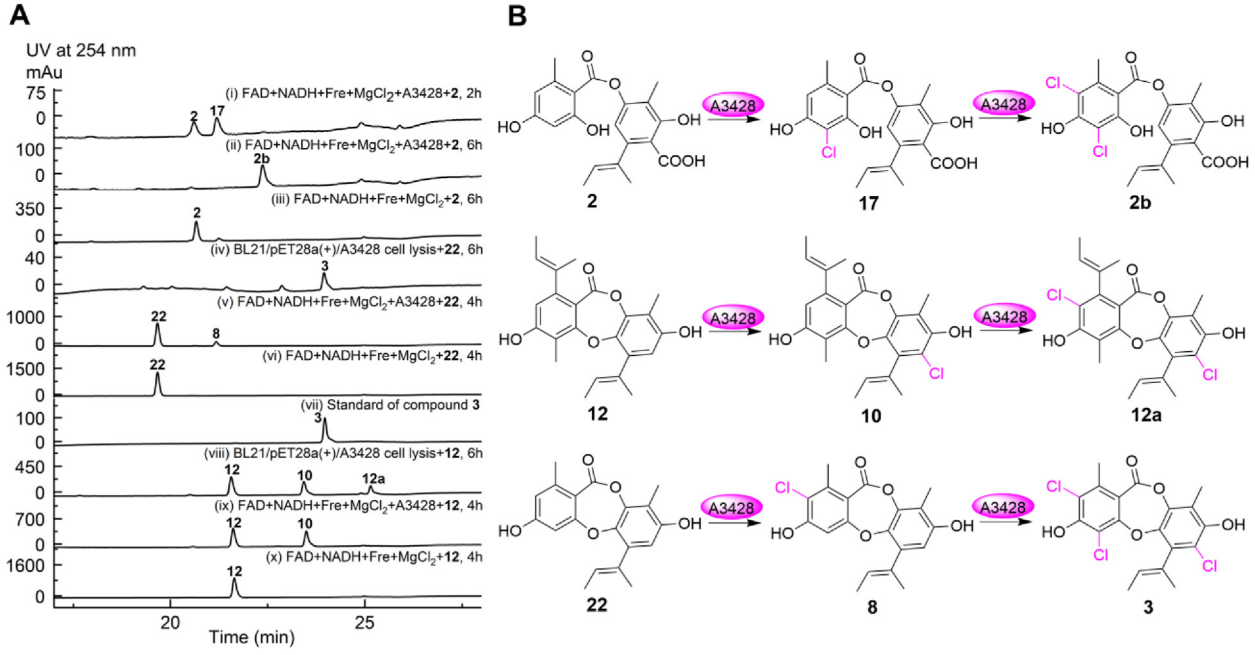

Figure 5 *In vitro* analysis of the flavin-dependent halogenase A3428. (A) HPLC traces of the A3428-catalyzed reactions; (B) The verified substrates and reactions catalyzed by A3428.

ning from 2 to 16 μg/mL (Supporting Information Table S2). Conversely, compounds **17**, **19**, and **21** displayed only weak anti-pathogenic activities with MIC values ≥ 32 μg/mL (Table S2). These results suggest that decarboxylated DEPs appear to have slightly superior antimicrobial activities relative to those bearing the C-1′ acid moiety. These findings support previously established SAR datasets[8].

3. Conclusions

Overall, the BGC encoding the DEPs was identified and characterized from our previously reported fungus *Aspergillus* sp. SCSIO SX7S7. Based on the CRISPR-Cas9 gene disruption system and heterologous expression experiments, we discovered that both hrPKS DepD and nrPKS DepH are indispensable to forming the precursor unguidepside A (**2**), which is distinct from previous depside formation. In addition, a CRISPR-Cas9-based gene disruption system and *in vitro* enzyme assays played essential roles in our elucidation of key tailoring steps involved in nornidulin (**3**) biosynthesis (Fig. 2D). The functions of three key tailoring enzymes were determined. The cytochrome P450 monooxygenase DepG converts the bicyclic depsides to tricyclic depsidones. The amidohydrolase superfamily protein DepF decarboxylates depsidone substrates, and finally, an uncommon flavin-dependent and remotely encoded halogenase A3428 catalyzes the multiple halogenations of depsides and depsidones. Coordinated with these efforts, we have also identified five new depside intermediates from an engineered Δ*depG* mutant, which exhibited moderate anti-pathogenic activities, indicating the potential of these molecules act as promising anti-infective drug lead compounds. Collectively, the discovery of the late-stage tailoring enzymes including DepF, DepG, and A3428, exhibit broad substrate promiscuity, which suggests their potential as genetic tools to expand DEP structural diversity. This study expands the foundation for future biosynthetic studies and bioengineering efforts to vastly enrich depsidone and depside structure libraries for initiatives in drug discovery and SM enzymology.

4. Experimental

4.1. General experimental procedures

U-2910 spectrometer (Hitachi) was used to record the UV spectra of compounds **17**−**21**. The 1D and 2D NMR spectra of compounds **17**−**21** were obtained with a Bruker Avance-700 spectrometer. All of the mass spectra were acquired on a Bruker MaXis Q-TOF mass spectrometer. Semi-preparative HPLC was performed on an Agilent 1260 HPLC system with a C_{18} column (YMC, 10 mm × 250 mm, 5 μm).

Strains and constructed plasmids utilized are shown in Supporting Information Tables S3−S4. LB medium was added with an additional antibiotic at a concentration of 50 μg/mL carbenicillin or 50 μg/mL kanamycin when necessary. Solid CD Medium was used for incubations of *A. nidulans* A1145 and *Aspergillus* sp. SCSIO SX7S7. The mutant strains of SCSIO SX7S7 were grown at Solid CD Medium with additional 200 μg/mL hygromycin (Hyg). Analytical or chromatographic-grade chemicals and solvents were used in this study.

4.2. DNA/RNA isolation, sequencing and manipulation

Genomic DNA from all fungal strains was prepared using lysis buffer (Supporting Information Table S6). Whole genome scanning of *Aspergillus* sp. SCSIO SX7S7 was finished using the 2nd generation Illumina sequencing platforms and 3rd generation PacBio RS (Shanghai Biozeron Biotechnology). The engineered yeast *Saccharomyces cerevisiae* JHY686-YH[27] was used to construct all of the *A. nidulans* A1154 ΔEM expression recombination plasmids.

Aspergillus sp. SCSIO SX7S7 was statically grown on PDB medium at 28 °C for 5 days and the mycelia were then collected. The total RNA was extracted from the mycelia following the manufacturer of the Coolaber® Fungal RNA Extraction Kit (Coolaber Technology, China) protocol. One-Step gDNA Removal and cDNA Synthesis SuperMix Kit (TransGen, China) was used to prepare the cDNA of SCSIO SX7S7.

4.3. Bioinformatic analysis

SM BGCs were analyzed using antiSMASH 6.0.0alpha software[16]. *Orfs* were assigned and their functions were predicted using FramePlot 4.0beta software, 2ndfiner software, and the BLAST program. MEGA 7.0 and ClustalX software were used to align the sequences.

4.4. HPLC analysis

The metabolites of *Aspergillus* sp. SCSIO SX7S7 and their mutants and *A. nidulans* A1145 were analyzed using an Agilent ZORBAX SB-C18 column (150 mm × 4.6 mm, 5 μm) with DAD detector under the solvent system (phase A, ddH_2O with 1‰ TFA; phase B, CH_3CN with 1‰ TFA): 0−20 min 5%−80% phase B; 20−23 min 80%−100% phase B; 23−27 min 100% phase B; 27−27.5 min 100%−0% phase B; 27.5−30 min 5% phase B; flow rate of 1 mL/min.

4.5. Preparation of protoplast A. nidulans A1154 and Aspergillus sp. SCSIO SX7S7 organisms

The general fungal transformation method has been previously described in detail elsewhere[27]. Briefly, for the transformation of A1145 and SCSIO SX7S7, spores were first grown on 50 mL liquid CD media which contains uridine (10 mmol/L), uracil (5 mmol/L), pyridoxine (0.5 μg/mL) and riboflavin (2.5 μg/mL) in a 250 mL flask at 28 °C, 200 rpm for about 12 h. Then, the germinated spores which were confirmed by microscopic examination were harvested and washed with 20 mL osmotic buffer (Supporting Information Table S6). Lysing enzyme (4 mg/mL, Sigma−Aldrich, Germany) and Yatalase (3 mg/mL, Takara, Japan) were used to prepare the protoplasts. Protoplasts were prepared by incubating the mixture in 10 mL osmotic buffer at 28 °C, 80 rpm for 10 h. The mixture was collected and transformed into a 30 mL sterile glass tube and overlaid carefully with 12 mL Trapping buffer (Supporting Information Table S6). After centrifugation (3900 rpm, 30 min, 4 °C), the protoplasts at the interface were carefully transformed into a 15 mL sterile tube and washed with 15 mL 1 × STC buffer (Table S6).

4.6. Construction of heterogenous expression strain

The heterologous expression plasmids were constructed using the plasmids pYTU (uracil used as an auxotrophic marker) and pYTP (pyridoxine used as an auxotrophic marker) as vectors to insert target genes[28].

For example, to construct the pYTU-depG plasmid, gene *depG* was amplified by PCR with a pair of primers of Recomb-pYTU-depG F1/R1 (Supporting Information Table S5). Then, the overlapping DNA fragment and the vector (digested by PacI and SwaI) were transformed into *S. cerevisiae* JHY686-YH for homologous recombination. Zymoprep™ Yeast Plasmid Miniprep Kit (Zymo Research, USA) was used to extract the plasmids in *S. cerevisiae* JHY686-YH and then introduced into *E. coli* DH5α by transformation. Recombined plasmids were sequenced to confirm identities. The remaining *A. nidulans* plasmids were generated following the same protocol of pYTU-depG. The resulting recombinant plasmids are listed in Table S2. For *A. nidulans* transformation, 1 μg pYTU-depG, 1 μg pYTP, and 1 μg pYTR were added to 70 μL protoplast and incubated on ice for 1 h. Next, 500 μL of PEG solution (Table S6) was added to the mixture for another 30 min and spread onto the CD-Sorbitol Medium (Table S6) and incubated at 28 °C until the transformants could be picked onto the CD-ST media (Table S6) for the production of heterologously expressed metabolites.

4.7. *Construction of CRISPR-Cas9 plasmids for fungal transformation*

The construction of our CRISPR-Cas9 plasmids has been previously described[17]. For further construction of plasmids used in the Cas9-based gene disruption system. Two overlapped fragments for overexpression of the single guide RNA (sgRNA) containing the target gene-specific protospacer sequence and the sgRNA scaffold sequence were amplified by PCR with two sets of primers of Cas9-sgDNA F/R and Cas9-depG F1/R1 (Supporting Information Table S5) using pFC332 as the template[29]. The fragments were inserted into the BsaI-digested pBSKII-Cas9-hph vector by Seamless Cloning and Assembly Kit (TransGen, China) and were introduced into commercial *E. coli* DH5α by transformation. Plasmids were then sequenced to confirm identities and named pCas9-depG. The remaining CRISPR-Cas9 gene disruption plasmids were generated following the same protocol of pCas9-depG. The gene-specific protospacer sequence was designed using an online website (http://zifit.partners.org/ZiFiT/ChoiceMenu.aspx).

4.8. *Gene disruption with CRISPR-Cas9 system*

The transformation of strain SCSIO SX7S7 was similar to the *A. nidulans* A1145 transformation described above. Briefly, 2.5 μg constructed CRISPR-Cas9 gene disruption plasmids listed in Table S3 were added to 75 μL *Aspergillus* sp. SCSIO SX7S7 protoplast suspension. Then 25 μL of PEG solution was added after blending and incubation on ice for 1 h. Subsequently, one milliliter of PEG solution was added for another 30 min at 28 °C and the mixture was spread onto CD Solid medium (Table S6) supplemented with 200 μg/mL hygromycin. Cultured onto CD agar medium (Table S6) supplemented with 200 μg/mL hygromycin at 28 °C until the transformants could be picked. Individual clones were validated by PCR amplified with proper primers flanking the target site.

4.9. *Preparation of microsomal fraction from the A1145-depG*

The A1145-depG strain harboring pYTU-depG was cultured in 30 mL CD-ST medium (28 °C, 200 rpm, 3 days). Then the mycelia were harvested and resuspended in A Buffer (Table S6). 100 μL zirconium silicate beads were added and broken in a bullet blender (Next Advance, USA) at 4 °C for 5 min. The homogenate was then centrifuged (14,000 rpm, 4 °C, 10 min) to remove the deposit. The supernatant was further fractionated by centrifugation at 14,000 rpm and 4 °C for 8 h. The microsome extracts were then resuspended in a total of 500 μL B Buffer (Table S6) and stored at −80 °C.

4.10. *Cloning, expression, and purification of A3428, DepF and Fre*

The gene for A3428/DepF from WT SCSIO SX7S7 cDNA was amplified by PCR with a pair of primers of pET28a-A3428/DepF-F1/R1 (Table S5) and cloned into the pET28a(+) overexpression vector (digested with NdeI and EcoRI). The sequence confirmed reconstruction plasmid of pET28a-A3428/DepF was used to transform to *E. coli* BL21(DE3) (TransGen, China) for overexpression of the A3428/DepF. The strain harboring pET28a-A3428/DepF was further cultured in 50 mL LB medium overnight and grown at 37 °C. Subsequently, two milliliters of BL21/pET28a-A3428/DepF culture was transferred into 500 mL LB medium for further incubation at 28 °C until the absorbance at 600 nm reached 0.3. Isopropylthio-β-D-galactoside (IPTG, 0.5 mmol/L) was used to induce the protein overexpression and the IPTG added culture was further incubated at 16 °C (160 rpm, 18 h). A total of 10 mL cells were harvested and resuspend in 25 mL lysis buffer (Table S6). The overexpressed A3428 and DepF were further purified using Qiagen Ni^{2+}-NTA affinity resin and eluted with buffer containing Tris-HCl (50 mmol/L), NaCl (300 mmol/L) and imidazole (300 mmol/L), pH 8.0. The crude extract containing A3428 or DepF was further purified by size-exclusion chromatography on a Superdex 200 column equilibrated in the storage buffer (Table S6). The flavin reductase enzyme (Fre) from *E. coli* BL21 (DE3) was also purified like protein A3428/DepF.

4.11. *Feeding experiments and in vitro* enzymatic reaction

The transformant strain *A. nidulans* A1145/depG was cultured on CD agar medium for 3 days as seed. The A1145/depG mycelia were then inoculated into 30 mL CD-ST medium with 1 mmol/L substrate dissolved in 100 μL DMSO after growing for 2 days. Subsequently, the transformant strain was cultured for an additional 24 h. The culture broth was collected and extracted with butanone for HPLC analysis.

A total of 500 μL reaction mixture, containing 427.5 μL microsomal fraction of the *A. nidulans* A1145/depG strain, 2 mmol/L NADPH, 100 mmol/L NaCl, and 0.1 mmol/L substrate was incubated at 30 °C for 24 h. Subsequently, the reaction mixture was extracted twice with EtOAc. After removal of solvent *in vacuo*, the extracted fraction was finally dissolved in methanol for HPLC and LC−HRESIMS analysis.

Purified DepF (20 μmol/L) was incubated with substrate (0.1 mmol/L) to a total volume of 100 μL at 30 °C with shaking at 300 rpm for 2 h in PBS buffer (10 mmol/L, pH 7.4). Purified A3428 (20 μmol/L) was incubated with Fre (10 μmol/L), FAD (10 μmol/L), NADH (2.5 mmol/L), $MgCl_2$ (25 mmol/L), DTT (0.1 mmol/L) and substrate (0.1 mmol/L) to a total volume of 100 μL at 30 °C for 4/12 h in PBS buffer (10 mmol/L, pH 7.4). Then added an equal amount of methanol and centrifugated to remove the precipitated protein. The supernate was directly used for HPLC and LC−HRESIMS analysis.

4.12. Determination of kinetic constants

To investigate the forward reaction kinetic constants of DepF, reaction mixtures were prepared in PBS buffer (10 mmol/L, pH 7.4) containing DepF (420 pmol/L for compound **2**, 4.5 nmol/L for compound **5**), and substrate (at 5, 10, 25, 50, 100, 200, 300, 400, and 500 μmol/L) in a total volume of 50 μL. Each reaction mixture was incubated at 30 °C for 8 min. The reaction was terminated by adding an equal amount of methanol. After centrifugation, the supernate was used for HPLC and LC−HRESIMS analysis. Activity data were evaluated by integrating HPLC analysis. Kinetic constants were generated by fitting these data to the Michaelis−Menten equation using Origin2017 software. Error bars were exhibited as SEM and calculated from three measurements.

4.13. Fermentation and isolation

The Δ*depG* mutant was placed onto CD agar medium containing 200 μg/mL Hyg at 28 °C for 5 days. Transferred the mycelium to PDB medium and incubated as seed cultures for 24 h (28 °C, 200 rpm). Subsequently, five milliliters of the seed culture were then inoculated into a 1 L flask (containing 200 mL PDB), shaking at 200 rpm for 7 days at 28 °C. After harvesting, a total of 12 L fermentation culture was centrifuged, and the mycelium cake and supernatant were extracted with acetone and butanone, respectively. The crude material mixture was subjected to a silica gel CC using a gradient of chloroform/methanol system (1:0 → 1:1, *v*/*v*) to afford a total of nine fractions (Frs. A1−A9). Frs. A1−A4 mixture was further purified by medium-pressure preparative liquid chromatography (ODS column, 40−63 μm, YMC), eluting with CH_3CN/H_2O (1:9 → 9:1, *v*/*v*) over 90 min at 15 mL/min, which afforded Frs. B1−B9. Frs. B3−B5 were further mixed and subjected to silica gel CC eluting with petroleum ether/chloroform gradient (1:0 → 0:1, *v*/*v*) to get 10 fractions (Frs. C1−C10). The compounds **17**−**21** were observed in Fr.C3. Compounds **17**−**21** were separated on YMC ODS-A semi-HPLC column with elution system (A: H_2O; B: CH_3CN): 0−27 min, 53%−85% phase B; 27−30 min, 53% phase B. As a result, compound **17** (16.7 mg, t_R = 15.2 min), compound **18** (8.7 mg, t_R = 16.1 min), compound **19** (5.4 mg, t_R = 18.0 min), compound **20** (19.4 mg, t_R = 19.0 min) and compound **21** (12.3 mg, t_R = 24.1 min) were purified.

4.14. Antipathogens activity assays

The antibacterial activities of compounds **17**−**21** were evaluated in this study using broth microdilution-based antimicrobial susceptibility tests for pathogens[30]. The tested Gram-positive bacteria were listed in Supporting Information Table S2.

4.15. Characterization of compounds

5-Chlorounguidepside (**17**): White power; UV (MeOH) λ_{max} (log ε) 215 (5.19), 273 (4.87), 308 (4.54) nm; ^{1}H and ^{13}C NMR data, see Tables S7 and S8; (−)-HRESIMS *m*/*z* 405.0756 $[M-H]^-$ (calcd. for $C_{20}H_{18}Cl_2O_7$, 405.0741).

5-Chlorodecarboxyunguidepside (**18**): White power; UV (MeOH) λ_{max} (log ε) 217 (5.74), 270 (5.36), 306 (4.93) nm; ^{1}H and ^{13}C NMR data, see Tables S7 and S8; (−)-HRESIMS *m*/*z* 361.0845 $[M-H]^-$ (calcd. for $C_{19}H_{18}ClO_5$, 361.0843).

3,5-Chlorounguidepside (**19**): White power; UV (MeOH) λ_{max} (log ε) 222 (5.50), 268 (5.08), 306 (4.93) nm; ^{1}H and ^{13}C NMR data, see Tables S7 and S8; (−)-HRESIMS *m*/*z* 439.0357 $[M-H]^-$ (calcd. for $C_{20}H_{17}Cl_2O_7$, 439.0351).

3,5-Chlorodecarboxyunguidepside (**20**): White power; UV (MeOH) λ_{max} (log ε) 217 (5.78), 254 (5.37), 319 (5.27) nm; ^{1}H and ^{13}C NMR data, see Tables S7 and S8; (−)-HRESIMS *m*/*z* 395.0465 $[M-H]^-$ (calcd. for $C_{19}H_{17}Cl_2O_5$, 395.0453).

3-Chloroagonodepside (**21**): White power; UV (MeOH) λ_{max} (log ε) 219 (5.90), 270 (5.42), 311 (5.17) nm; ^{1}H and ^{13}C NMR data, see Tables S7 and S8; (−)-HRESIMS *m*/*z* 459.1220 $[M-H]^-$ (calcd. for $C_{24}H_{24}ClO_7$, 459.1211).

Acknowledgments

This research was funded by the National Natural Science Foundation of China (22037006, U2106207, 22077128), Local Innovation and Entrepreneurship Team Project of Guangdong (2019BT02Y262, China), Key Science and Technology Project of Hainan Province (ZDKJ202018, China), Major Project of Basic and Applied Basic Research of Guangdong Province (2019B030302004, China), Key-Area Research and Development Program of Guangdong Province (2020B1111030005, China), Guangdong Provincial Marine Economic Development (Six Major Marine Undertakings, China) Special Fund Project (GDNRC[2021]54, China) and Open Program of Shenzhen Bay Laboratory (SZBL2021080601006, China). We thank The Analytical Facility Center of the South China Sea Institute of Oceanology. In particular, we acknowledge Dr. Zhihui Xiao and Dr. Xiaohong Zheng for recording NMR data, Ms. Aijun Sun, Ms. Yun Zhang, and Ms. Xuan Ma for acquiring HRESIMS data.

Author contributions

Jianhua Ju and Yongxiang Song designed research; Jiafan Yang and Zhenbin Zhou performed research; Jiafan Yang, Zhenbin Zhou, Yingying Chen, Yongxiang Song and Jianhua Ju analyzed data; Jiafan Yang, Yingying Chen and Jianhua Ju wrote the manuscript.

Conflicts of interest

The authors declare no conflicts of interest.

Appendix A. Supporting information

Supporting data to this article can be found online at https://doi.org/10.1016/j.apsb.2023.05.036.

References

1. Ibrahim SRM, Mohamed GA, Al Haidari RA, El-Kholy AA, Zayed MF, Khayat MT. Biologically active fungal depsidones: chemistry, biosynthesis, structural characterization, and bioactivities. *Fitoterapia* 2018;**129**:317−65.
2. Duong TH, Hang TX, Pogam PL, Tran TN, Mac DH, Dinh MH, et al. α-Glucosidase inhibitory depsidones from the lichen *Parmotrema tsavoense*. *Planta Med* 2020;**86**:776−81.
3. Sukandar ER, Siripong P, Khumkratok S, Tip-Pyang S. New depsidones and xanthone from the roots of *Garcinia schomburgkiana*. *Fitoterapia* 2016;**111**:73−7.

4. Zwartsen A, Chottanapund S, Kittakoop P, Navasumrit P, Ruchirawat M, Van Duursen MBM, et al. Evaluation of anti-tumour properties of two depsidones−Unguinol and Aspergillusidone D−in triple-negative MDA-MB-231 breast tumour cells. *Toxicol Rep* 2019; **6**:1216−22.
5. Bay MV, Nam PC, Quang DT, Mechler A, Hien NK, Hoa NT, et al. Theoretical study on the antioxidant activity of natural depsidones. *ACS Omega* 2020;**5**:7895−902.
6. Urena-Vacas I, Gonzalez-Burgos E, Divakar PK, Gomez-Serranillos MP. Lichen depsidones with biological interest. *Planta Med* 2021;**88**:855−80.
7. Morshed MT, Vuong D, Crombie A, Lacey AE, Karuso P, Lacey E, et al. Expanding antibiotic chemical space around the nidulin pharmacophore. *Org Biomol Chem* 2018;**16**:3038−51.
8. Yang JF, Zhou L, Zhou ZB, Song YX, Ju JH. Anti-pathogenic depsidones and its derivatives from a coral-derived fungus *Aspergillus* sp. SCSIO SX7S7. *Biochem Systemat Ecol* 2022;**102**:104415−9.
9. Arquie E, Grumbach F, Boyer F, Sanchez G. A new antibiotic produced by a strain of *Sterygmatocystis nidulans*, nidulin. *C R Hebd Seances Acad Sci* 1949;**229**:602−4.
10. Chen L, Wei X, Matsuda Y. Depside bond formation by the starter-unit acyltransferase domain of a fungal polyketide synthase. *J Am Chem Soc* 2022;**144**:19225−30.
11. Wei Q, Wang ZP, Zhang X, Zou Y. Diaryl ether formation by a versatile thioesterase domain. *J Am Chem Soc* 2022;**144**:9554−8.
12. Liu Q, Zhang D, Gao S, Cai X, Yao M, Xu Y, et al. Didepside formation by the nonreducing polyketide synthase Preu6 of *Preussia isomera* requires interaction of starter acyl transferase and thioesterase domains. *Angew Chem Int Ed Engl* 2022:e202214379.
13. Isaka M, Yangchum A, Supothina S, Veeranondha S, Komwijit S, Phongpaichit S. Semisynthesis and antibacterial activities of nidulin derivatives. *J Antibiot* 2019;**72**:181−4.
14. Morshed MT, Nguyen HT, Vuong D, Crombie A, Lacey E, Ogunniyi AD, et al. Semisynthesis and biological evaluation of a focused library of unguinol derivatives as next-generation antibiotics. *Org Biomol Chem* 2021;**19**:1022−36.
15. Banik JJ, Craig JW, Calle PY, Brady SF. Tailoring enzyme-rich environmental DNA clones: a source of enzymes for generating libraries of unnatural natural products. *J Am Chem Soc* 2010;**132**: 15661−70.
16. Blin K, Shaw S, Kloosterman AM, Charlop-Powers Z, van Wezel GP, Medema MH, et al. antiSMASH 6.0: improving cluster detection and comparison capabilities. *Nucleic Acids Res* 2021;**49**:W29−35.
17. Chen YY, Cai CL, Yang JF, Shi JJ, Song YX, Hu D, et al. Development of the CRISPR-Cas9 system for the marine-derived fungi *Spiromastix* sp. SCSIO F190 and *Aspergillus* sp. SCSIO SX7S7. *J Fungi* 2022;**8**:715−29.
18. Chiang YM, Lin TS, Wang CCC. Total heterologous biosynthesis of fungal natural products in *Aspergillus nidulans*. *J Nat Prod* 2022;**85**: 2484−518.
19. Feng C, Wei Q, Hu CH, Zou Y. Biosynthesis of diphenyl ethers in fungi. *Org Lett* 2019;**21**:3114−8.
20. Seibert CM, Raushel FM. Structural and catalytic diversity within the amidohydrolase superfamily. *Biochemistry-Us* 2005;**44**:6383−91.
21. Sheng X, Cai CL, Yang JF, Shi JJ, Song YX, Hu D, et al. Mechanism and structure of γ-resorcylate decarboxylase. *Biochemistry* 2018;**57**: 3167−75.
22. Hult K, Berglund P. Enzyme promiscuity: mechanism and applications. *Trends Biotechnol* 2007;**25**:231−8.
23. Khersonsky O, Tawfik DS. Enzyme promiscuity: a mechanistic and evolutionary perspective. *Annu Rev Biochem* 2010;**79**:471−505.
24. Menon BRK, Brandenburger E, Sharif HH, Klemstein U, Shepherd SA, Greaney MF, et al. RadH: a versatile halogenase for integration into synthetic pathways. *Angew Chem Int Ed Engl* 2017; **56**:11841−5.
25. Tsunematsu Y, Maeda N, Yokoyama M, Chankhamjon P, Watanabe K, Scherlach K, et al. Enzymatic amide tailoring promotes retro-aldol amino acid conversion to form the antifungal agent aspirochlorine. *Angew Chem Int Ed Engl* 2018;**57**:14051−4.
26. Spyrou G, Haggard-Ljungquist E, Krook M, Jornvall H, Nilsson E, Reichard P. Characterization of the flavin reductase gene (*fre*) of *Escherichia coli* and construction of a plasmid for overproduction of the enzyme. *J Bacteriol* 1991;**173**:3673−9.
27. Yan Y, Liu QK, Zang X, Yuan SG, Bat-Erdene U, Nguyen C, et al. Resistance-gene-directed discovery of a natural-product herbicide with a new mode of action. *Nature* 2018;**559**:415−8.
28. Yan Y, Zang X, Jamieson CS, Lin HC, Houk KN, Zhou JH, et al. Biosynthesis of the fungal glyceraldehyde-3-phosphate dehydrogenase inhibitor heptelidic acid and mechanism of self-resistance. *Chem Sci* 2020;**11**:9554−62.
29. Nodvig CS, Nielsen JB, Kogle ME, Mortensen UH. A CRISPR-Cas9 system for genetic engineering of filamentous fungi. *PLoS One* 2015; **10**:e0133085.
30. Yang JF, Song YX, Tang MC, Li MZ, Deng JW, Wong NK, et al. Genome-directed discovery of tetrahydroisoquinolines from deep-sea derived *Streptomyces niveus* SCSIO 3406. *J Org Chem* 2021;**86**:11107−16.